J Mater Sci (2008) 43:1890–1896
DOI 10.1007/s10853-007-2419-7

Implantable photonic crystal for reflection-based optical sensing of biodegradation

Musashi Fujishima · Syoei Sakata · Takuya Iwasaki · Kumao Uchida

Received: 24 September 2007 / Accepted: 21 December 2007 / Published online: 31 January 2008

Abstract Biodegradable inverse opal (IoPPC) was synthesized from a multifunctional carboxylic acid and polyols by colloidal crystal templating. The IoPPC was prepared by infiltration of the monomer solution into interparticle voids of silica colloidal crystal template, polycondensation of the infiltrated film, and removal of the template. The synthesized IoPPC was characterized by infrared absorption, X-ray diffraction measurements, differential scanning calorimetry, and thermogravimetry/mass spectrometry analysis. In order to clarify the effect of biodegradation on the inverse opal structure and the optical reflection property, the IoPPC was implanted in subcutaneous tissue of the lower back of three mice (ICR, 10 weeks, female). After the 2 weeks implantation, fragmented samples were harvested from the implant location and investigated by scanning electron microscope observations and optical reflection measurements. It was found that the reflection peak for the harvested samples decayed from that for the sample without implantation. Such a spectral change is considered to be attributed to the deterioration of the regularity of the inverse opal structures through biodegradation. The finding of this study will serve in the development of reflection-based sensing in various biomedical applications.

The in vivo degradation experiment was approved by the committee on animal experiments of School of Science and Engineering, Kinki University.

M. Fujishima (✉) · S. Sakata · T. Iwasaki · K. Uchida
School of Science and Engineering, Kinki University,
3-4-1 Kowakae, Higashi-Osaka, Osaka 577-8502, Japan
e-mail: mfujishima@apch.kindai.ac.jp

Introduction

Biodegradable materials with three-dimensional porous structures are of great interest because of a wide variety of potential biomedical applications. Many types of fabrication techniques such as salt leaching, freeze drying [1], phase separation [2], foaming [3], molding [4–9] are presently used to prepare scaffolds for cell culture, artificial organs, and microchip devices for drug delivery systems (DDS) [10, 11]. For all of these applications, regulation of the pore geometry, i.e., porosities, pore sizes, and pore arrangements, is very important because it affects the characteristics of the materials such as mechanical strength, thermal stability, degradability, cell affinity, adsorptive activity, and release ability of the adsorbates.

Among the fabrication techniques, colloidal crystal templating has attracted much attention because it enables the fabrication of periodic porous structures, so-called inverse opal structures, from various kinds of organic and inorganic materials [12, 13]. Inverse opals are fabricated by following facile procedures: infiltration of the solution of monomers (or preformed polymers) or sol-gel precursors into interparticle voids of the colloidal crystal template, polymerization of the monomers or evaporation of solvents from the infiltrated template, and removal of the template by etching or calcination. The fabricated inverse opal structures possess solid frameworks that divide the internal space into three-dimensional periodic arrays of pores with controlled sizes.

The inverse opals are considerably different from porous materials prepared from conventional techniques. They are three-dimensional photonic crystals displaying characteristic structural color. The colorization is derived from the Bragg diffraction that occurs when the periodicity of their

structures is comparable to the wavelength of visible or near infrared (NIR) light [14]. In recent years, inverse opals with this optical property have been studied for use for reflection-based optical sensing of pH [15], temperature [16], biochemical reaction [17], and metal ions [18]. From the viewpoint of biomedical applications, inverse opals made up of biodegradable polymers have a bright prospect of becoming novel implantable porous materials that may enable reflection-based optical sensing of biodegradation. However, there have been few reports of such inverse opals [19].

In this paper, we report the biodegradable inverse opal (IoPPC) that has the potential of becoming implantable three-dimensional photonic crystals. The interesting feature is that the inverse opal in this study shows the selective NIR reflection, intensity of which varies with biodegradation because of the simultaneous destruction of the porous structures. It is well known that living tissues are relatively transparent in the NIR region around 650–1,100 nm because the absorbance of H_2O and hemoglobin, which are the main absorbers of light in living tissue, is very low in this region [20]. Therefore, the inverse opal will be, in principle, visible even under implanted conditions in living tissue. Furthermore, the inverse opal does not require surgical removal from the implant location at the completion of use because it can completely degrade in physiological environments. Based on these functionalities, IoPPCs will enable reflection-based optical sensing for events such as release of loaded drugs [21, 22], proliferation of cultured tissues, and bioresorption when used as artificial organs.

Among many kinds of biodegradable polymeric materials [23], we have focused on citric acid-based polyesters composed of multifunctional carboxylic acids and polyols [24, 25]. The polyesters are biodegradable elastomers having regular network structures formed by cross-linkages among the monomers by ester bonds. They can be synthesized by a facile synthetic process without expensive monomers, harmful catalysts, and cross-linking reagents. Their physicochemical properties including elasticity can be controlled by synthetic parameters such as temperature, reaction period, concentration, and monomer composition.

Here, we report synthesis, characterization, and evaluation of the optical reflection property of the IoPPC. The effect of in vivo biodegradation on the inverse opal structure and the optical reflection is firstly presented. In the degradation experiments, sample films were implanted in subcutaneous tissue of mice (ICR, 10 weeks, female). We selected the lower back of mice as an implant location in order to protect implanted samples from self-injurious behavior in mice and to evaluate the sole effect of biodegradation.

Experimental

Preparation of colloidal crystal template

Colloidal crystal templates were prepared by a gravity sedimentation method modified from one previously reported [26, 27]. Several drops of 10 wt.% colloidal dispersions of silica microspheres with an average diameter of 300 nm (Polysciences, Inc.) were placed on glass substrates and left in an airtight container for several days at room temperature. In this process, solvents of the dispersions were allowed to completely evaporate and then iridescent templates were formed.

Synthesis of IoPPC

All reagents for the synthesis of the citric acid-based polyester, poly(1,5-pentanediol-co-pentaerythritol-co-citric acid) (PPC) were purchased from Wako Chemicals, Inc. The mixed aqueous solution of citric acid, 1,5-pentanediol, and pentaerythritol with a molar ratio of 12:10:1 was infiltrated into the voids of the templates and the excess solution was carefully removed from the template surfaces. The infiltrated films were settled in the pressure bottles with a few droplets of deionized water and then kept in an oven at 127 °C for 1 day. During this procedure, vapor pressure was exerted on the films and the generation of air bubbles over the polycondensation of the monomers was suppressed. The cured composite films were immersed in an etching solution composed of dimethyl sulfoxide, 42% aqueous solution of ammonium fluoride, and ethanol for up to 48 h. By this treatment, the templates were completely dissolved. The remaining iridescent films were rinsed with deionized water several times and stored in ethanol.

Microscope observation

Structural color of IoPPC was observed with an optical microscope (Nikon, LV100D). Scanning electron microscope (SEM) images were taken with a field emission SEM (Hitachi High-Technologies, S-4800). Before the SEM observations were taken, the samples were lyophilized and sputtered with Os vapor. The composition of the samples was also determined by energy dispersive X-ray spectroscopy (EDS) using an EDS analyzer (HORIBA, EMAX ENERGY EX-250) combined with SEM.

Characterization

The IoPPC at an etching time of 48 h was used for characterization. Fourier transformed infrared (FTIR)

absorption was recorded at room temperature using an FTIR spectrometer (JASCO, FT/IR-470). X-ray diffraction (XRD) measurement was performed with an X-ray diffractometer (Bruker AXS, D8 Advance) with Cu Kα radiation. Differential scanning calorimetry (DSC) thermogram was obtained on a differential scanning calorimeter (Shimadzu, DSC-60) under an N_2 gas atmosphere. Measurements were carried out in the range of −50 to 100 °C with a heating rate of 10 °C/min. Before the thermograms were recorded, the samples were preheated from room temperature to 100 °C and cooled to −50 °C with heating and cooling rates of 10 °C/min. The glass transition temperature was determined as the starting point of the recorded step change in heat capacity. The thermal stability of IoPPC was evaluated by thermogravimetry/mass spectrometry (TG/MS) analysis with a Bruker TG-DTA/M59610 in the temperature range of 30 to 400 °C. In the experiments, temperature dependence of the ionic currents from decomposition products (H_2O and CO_2) was monitored during the heating.

Evaluation of optical property

UV–Vis–NIR absorption spectrum was recorded at room temperature using a UV/VIS/NIR spectrophotometer (JASCO, V-570). Reflection spectra were obtained at normal incidence to the samples using an optical microscope combined with a fiber optic spectrometer (Ocean Optics, HR4000-CG). An objective lens (10× / 0.3 N.A.) and an optical fiber with a diameter of 1 mm were used for the measurements. The refractive index of PPC was determined by a multiwavelength Abbe refractometer (ATAGO, DR-M2) with an interference filter of 689 nm at 25 °C.

In vivo degradation study

In vivo degradation experiments were performed by subcutaneous implantation of sample films in the lower backs of three mice (ICR, 10 weeks, female). The films were rinsed with saline prior to the implantation, and then inserted in the subcutaneous tissue for 2 weeks. At the end of the implantation period, fragmented films were harvested from the implant location and rinsed with saline and ethanol several times, and then stored in a glass bottle filled with ethanol. In order to certify the biocompatibility of the implanted samples, weights of mice were measured during the implantation period. Survival of mice after the completion of the implant experiments was confirmed.

Results and discussion

Microscope observation of IoPPC

Figure 1a is a photograph of IoPPC at an etching time of 48 h, which was obtained at normal incidence of white light with respect to the sample surface. IoPPC appeared brilliant red under immersion in deionized water. Since non-porous PPC has no apparent absorption in the visible region, such colorization should be caused by optical diffraction by the inverse opal structure. The irregular lines observed in the photograph are assumed to be caused by the replication of crevices in the template.

Figure 2 shows SEM images of the colloidal crystal template, the composite film, and the etched IoPPC at a various etching time. The image of the template (Fig. 2a) shows a hexagonally close-packed array of uniform microspheres (mean diameter 300 nm). The direction

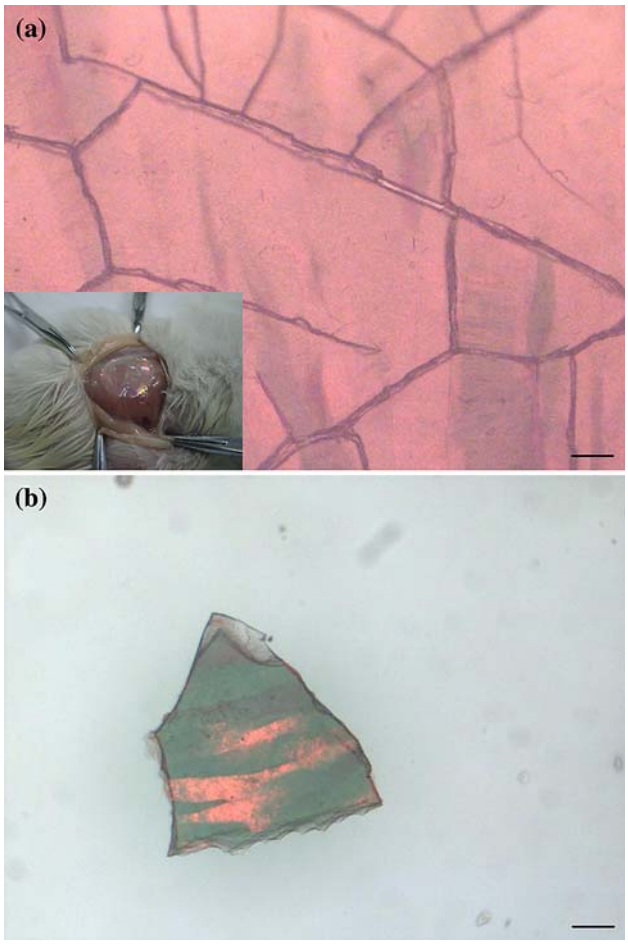

Fig. 1 Optical microscope images of (**a**) IoPPC (etching time: 48 h) and (**b**) harvested IoPPC from mouse after subcutaneous implantation (scale bar: 100 μm). The samples were immersed in deionized water and illuminated with a white light from normal with respect to the sample surfaces. Inset in (a): photograph of the IoPPC implanted in subcutaneous tissue of mouse

vertical to the image corresponds to the (111) direction of the face-centered cubic (fcc) lattice. From the image of the composite film (Fig. 2b), the voids of the templates seems to be occupied completely with PPC.

Figure 2c shows IoPPC at an etching time of 5 h, in which the periodic pore arrays were observed. This suggests that the close-packed fcc structure of the template was successfully replicated in PPC. Residues in the pores seemed to be silica colloids, which were removed by further etching. From EDS analysis for the IoPPC at an etching time of 30 and 48 h (Fig. 2d, e), no signal from either Si or F was detected indicating the completion of the removal of the template and the etching solution.

It can be seen that the further etching caused collapse of pores and distortion of their arrangement on these samples (Fig. 2d, e). In addition, the etched samples did not show any structural color in lyophilized condition for the SEM observations, whereas they did in wet condition (Fig. 1a). The observed deformation of the porous structure and disappearance of the color should come from the fact that IoPPC is a hydrogel that becomes contracted by removal of the water absorbed within the network structure. Identification of the hydrogel structure is discussed in the following section.

Characterization of IoPPC

The FTIR spectrum (Fig. 3) showed an intense absorption peak between 1,690 and 1,770 cm^{-1}, which can be assigned to the C=O stretching mode. The broadening of this peak implies the existence of C=O bonds in residual carboxyl groups in addition to the existence of C=O bonds in ester bond. It also suggests that these C=O bonds take part in the formation of the intramolecular hydrogen bond. The hydrogen bonding is also confirmed by the broad absorption peaks of O–H stretching mode at 3,235 and 3,480 cm^{-1}.

The XRD pattern of IoPPC (Fig. 4) showed a broad intense diffraction peak at $2\theta = 19.7°$. According to the literature [28], such peak is attributed to a regular network

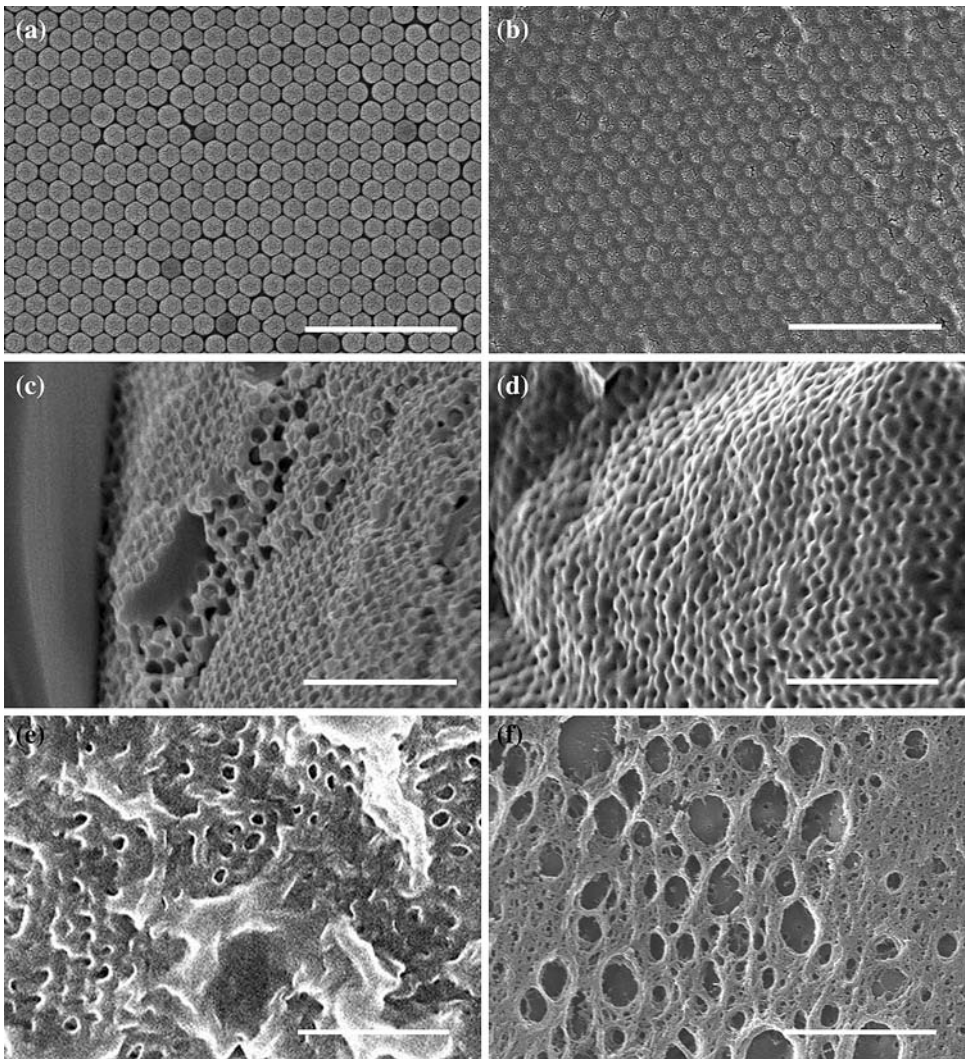

Fig. 2 SEM images of (**a**) colloidal crystal template, (**b**) composite film, and IoPPC at an etching time of (**c**) 5, (**d**) 30, (**e**) 48 h, and (**f**) harvested IoPPC from mouse after subcutaneous implantation (scale bars: 2 μm)

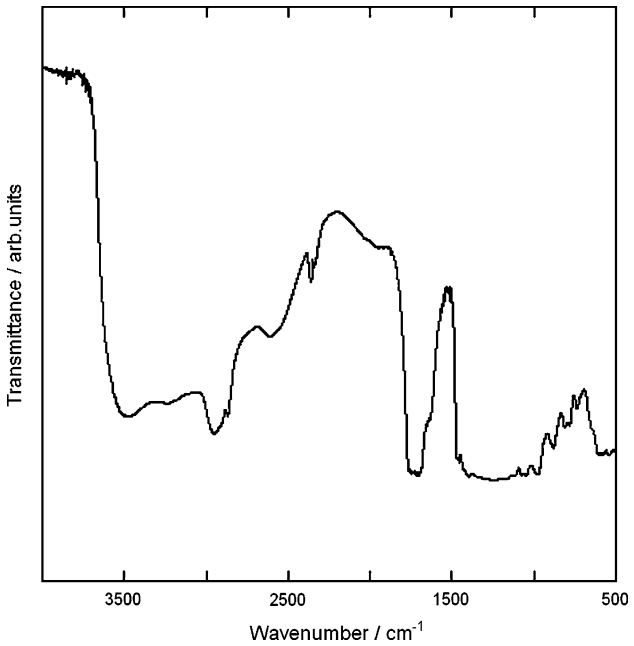

Fig. 3 FTIR absorption spectrum of IoPPC (etching time: 48 h)

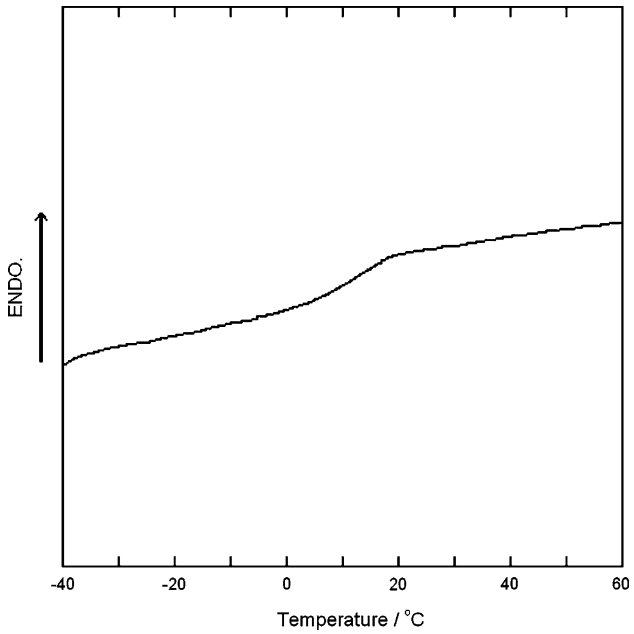

Fig. 5 DSC thermogram of IoPPC (etching time: 48 h)

structure formed by esterification among multifunctional monomers with symmetric molecular structure. The d-spacing of this structure was calculated to be 4.5 Å.

Differential scanning calorimetry thermogram in Fig. 5 showed endothermic change at 3.8 °C indicating glass transition temperature. A similar thermal behavior is frequently observed for aliphatic polyesters composed of multifunctional monomers [25, 28]. In addition, no crystallization or melting peaks of the monomers were observed in the thermogram, suggesting complete esterification of the monomers.

The thermal stability of IoPPC was investigated by TG/MS analysis. As shown in Fig. 6, the increase in ionic currents from H_2O and CO_2 was observed at ca. 230 °C, indicating the decomposition of IoPPC. Moreover, the ionic current from H_2O showed a broad peak at 128 °C.

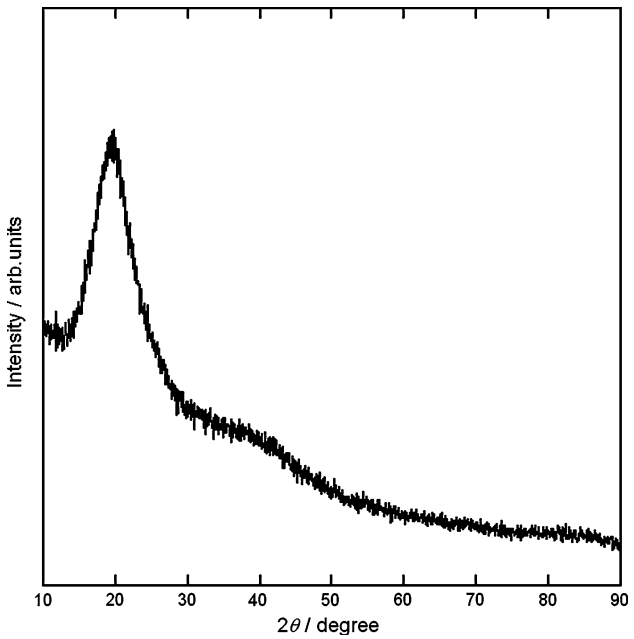

Fig. 4 XRD pattern of IoPPC (etching time: 48 h)

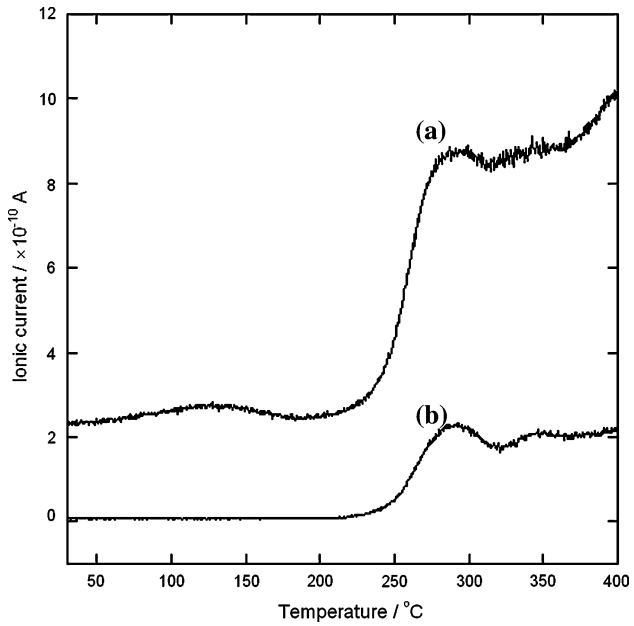

Fig. 6 Temperature dependence of ionic currents for IoPPC (etching time: 48 h). Curves correspond to ionic currents from (**a**) H_2O and (**b**) CO_2, respectively

This should come from the release of the water absorbed within the hydrophilic network structure.

Optical reflection property of IoPPC

Figure 7a shows the reflection spectrum obtained with IoPPC under immersion in deionized water. The reflection spectrum of a colloidal crystal template in air is also displayed. The maximum reflection wavelength, λ_{max}, for the IoPPC is 679 nm. From this value, the pore diameter of the IoPPC was estimated by a modified version of the Bragg equation, as follows [29–31]:

$$\lambda_{max} = 2(d/m)n_s^2 V_s + n_f^2 V_f - \sin^2\theta)^{1/2}, \quad (1)$$

where d is the interplanar spacing, m is the order of the Bragg diffraction, n is the refractive index, V is the volume fraction, and θ is the incident angle of light measured from the sample normal. (Subscripts s and f mean sphere and framework, respectively.)

For an fcc lattice, the relationship between the interplanar spacing d and the center-to-center distance D between spheres is given by the following equation:

$$d = 2^{1/2}D/(h^2 + k^2 + l^2)^{1/2}. \quad (2)$$

Assuming that the optical reflection is derived from the (111) planes, we obtained the d value, $0.8165D$. Combining Eq. 1 with Eq. 2 gives the following contracted expression:

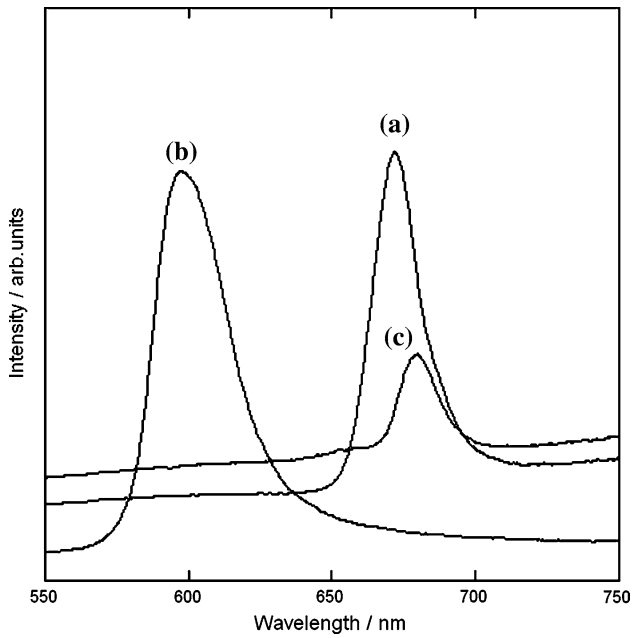

Fig. 7 Optical reflection spectra of (**a**) IoPPC (etching time: 48 h), (**b**) colloidal crystal template, and (**c**) harvested IoPPC from mouse after subcutaneous implantation. Spectra were obtained at normal incidence of white light to the IoPPC and harvested IoPPC immersed in deionized water, and the template in air

$$\lambda_{max} = 1.633(D/m)(n_s^2 V_s + n_f^2 V_f - \sin^2\theta)^{1/2}. \quad (3)$$

From Eq. 3, the pore diameter of the IoPPC in wet condition was estimated to be 303 nm using values of $V_s = 0.74$, $V_f = 0.26$, $m = 1$, $\theta = 0$, and refractive indexes of water ($n_s = 1.33$) and PPC ($n_f = 1.49$). Since the estimated value is in reasonable agreement with the mean diameter of silica spheres (300 nm), it can be mentioned that the fcc geometry of the template was completely transferred into the inverse opal structure and is sustained under immersion in deionized water.

The optical reflection of the IoPPC is appreciably different from that of the template (Fig. 7b) in the peak position and peak width. The spectral difference is derived from the difference in the average refractive index (n_a) and the refractive index contrast (n_c) [32]. In brief, the peak position shifts toward lower energy with an increase in n_a, and the peak width becomes narrower with a decrease in n_c. In the present case, these trends are achieved for the IoPPC in wet condition ($n_a = 1.37$, $n_c = 0.16$) and the template in air ($n_a = 1.22$, $n_c = 0.29$) [33].[1]

Modulation of optical reflection property by biodegradation

Preliminary experiments were performed in order to examine the effect of biodegradation on the inverse opal structure and the optical reflection property. As shown in the inset of Fig. 1a, the sample films were implanted in the subcutaneous tissue of the lower back of mice for 2 weeks. Since the mice showed no remarkable weight loss during the implantation period and survived after that, it can be said that the IoPPC is biocompatible. Figure 1b is a photograph of the harvested IoPPC from one of the mice, in which brilliant red observed for the original sample (Fig. 1a) appears to be faded. The fading of the color is supposed to be due to the overlap of colors of the degraded IoPPC (pale brown) and the view field of the optical microscope (pale blue). The harvested sample was observed to be broken into small fragments. The fragmentation could result from degradation along the replicated crevices as shown in Fig. 1a. Figure 2f shows an SEM image of the harvested sample, where irregular porous structure with non-uniform pores was observed instead of the replicated pores as shown in Fig. 2e. Such irregular structure seems to be responsible for the fading of the color.

[1] The refractive index of silica colloids was estimated to be 1.29 from Eq. 3 with a λ_{max} value of 597 nm (Fig. 7b). Such a small refractive index as compared with the value of crystalline silicon dioxide (1.45) is derived from the mesoporous structure of the silica colloids.

Figure 7c shows the reflection spectrum for a piece of the harvested fragments. It can be seen that the reflection peak for the piece decayed from that for the sample without implantation (Fig. 7a). Although the extent of the decay varied from piece to piece because of differences in the degree of biodegradation under heterogeneous in vivo environment, the trend of the decay was confirmed for each piece. Such a spectral change is considered to be attributed to the deterioration of the regularity through biodegradation, which leads to the reduction of number of lattice planes required for the Bragg diffraction of incident light. These preliminary results suggest that IoPPC has an ability to inform observers of its own degradation by changing its optical reflection.

Such degradation-dependent reflection property is expected to be applied to reflection-based optical sensing in DDD, tissue engineering, and artificial organs. Although the utilization of the inverse opal of this study is restricted only in wet condition because of the contractive polymer frameworks, it will expand through the improvement of the structural robustness of the frameworks. Robustness is considered to be improved by an increase in the number of cross-linkages between monomers through the regulation of synthetic parameters. Another way of fabricating robust IoPPCs should be the use of crystalline polymers, e.g., poly(lactic acid) and cellulose, as additives. Studies for these methods are now in progress.

Conclusion

Biodegradable inverse opal with optical reflection property was successfully synthesized from a multifunctional carboxylic acid and polyols by colloidal crystal templating. This is the first example of implantable three-dimensional photonic crystals that can inform observers of its own degradation by changing its optical reflection. The results of this study should contribute to develop reflection-based optical sensing in various biomedical applications.

Acknowledgements The authors thank H. Kitagawa of Kyushu University for XRD measurements and TG/MS analyses. We also acknowledge R. Moriyama of Kinki University for technical instruction in the animal experiments. This work was partly supported by a grant-in-aid for Scientific Research (No. 18500369) from the Ministry of Education, Culture, Sports, Science and Technology, and by the Circle for the Promotion of Science and Engineering.

References

1. Karageorgiou V, Kaplan D (2005) Biomaterials 26:5474
2. Hua FJ, Kim GE, Lee JD, Son YK, Lee DS (2002) J Biomed Mater Res 63:161
3. Harris LD, Kim BS, Mooney DJ (1998) J Biomed Mater Res 42:396
4. Ma PX, Choi JW (2001) Tissue Eng 7:23
5. Marshall AJ, Ratner BD (2005) AIChE J 51:1221
6. Ratner BD, Marshall AJ (2006) Polym Prepr 47:69
7. Zhang K, Yan H, Stein A, Francis LF (2005) J Am Ceram Soc 88:587
8. Zhang K, Yan H, Bell DC, Stein A, Francis LF (2003) J Biomed Mater Res 66A:860
9. Yan H, Zhang K, Blanford CF, Francis LF, Stein A (2001) Chem Mater 13:1374
10. Grayson CR, Choi IS, Tyler BM, Wang PP, Brem H, Cima MJ, Langer R (2003) Nat Mater 2:767
11. Levenberg S, Langer R (2004) Curr Top Dev Biol 61:113
12. Xia Y, Gates B, Yin Y, Lu Y (2000) Adv Mater 12:693
13. Stein A, Schroden RC (2001) Curr Opin Solid-State Mater Sci 5:553
14. Diop M, Lessard RA (2003) J Nonlinear Opt Quantum Opt 30:203
15. Lee YJ, Braun PV (2003) Adv Mater 15:563
16. Takeoka Y, Watanabe M (2003) Adv Mater 15:199
17. Cassagneau T, Caruso F (2002) Adv Mater 14:1629
18. Liu J, Li G, Wu Z, An Q, Qiu Y (2007) ChemPhysChem 8:1298
19. Fujishima M, Sakata S, Kikoku M, Ogawa D, Uchida K (2007) Chem Lett 36:1510
20. Weissleder R (2001) Nat Biotechnol 19:316
21. Li YY, Cunin F, Link JR, Gao T, Betts RE, Reiver SH, Chin V, Bhatia SN, Sailor MJ (2003) Science 299:2045
22. Dupuis A, Guo N, Gao Y, Godlbout N, Lacroix S, Dubois C, Skorobogatiy M (2007) Opt Lett 32:109
23. Ikada Y, Tsuji H (2000) Macromol Rapid Commun 21:117
24. Yang J, Webb AR, Ameer GA (2004) Adv Mater 16:511
25. Yang J, Webb AR, Pickerill SJ, Hageman G, Ameer GA (2006) Biomaterials 27:1889
26. Denkov ND, Velev OD, Kralchevsky PA, Ivanov IB, Yoshimura H, Nagayama K (1993) Nature 361:26
27. Míguez H, Meseguer F, López C, Mifsud A, Moya JS, Vázquez L (1997) Langmuir 13:6009
28. Nagata M, Kono Y, Sakai W, Tsutsumi N (1999) Macromolecules 32:7762
29. Schroden RC, Al-Daous M, Blanford CF, Stein A (2002) Chem Mater 14:3305
30. Blanford CF, Schroden RC, Al-Daous M, Stein A (2001) Adv Mater 13:26
31. Richel A, Johnson NP, McComb DW (2000) App Phys Lett 76:1816
32. Míguez H, Meseguer F, López C, Lopez-Tejeira F, Sanchez-Dehesa J (2001) Adv Mater 13:393
33. Busch K, John S (1998) Phys Rev E 58:3896